Journal of Inflammation Research Dovepress

Open Access Full Text Article ORIGINAL RESEARCH

IRGM Deficiency Exacerbates Sepsis-Induced Acute Lung Injury by Inhibiting Autophagy Through the AKT/mTOR Signaling Pathway

Na Guo[1,*], Yu Xia[1,*], Nannan He[1], Huixin Cheng[1], Lei Zhang[2], Jian Liu[1,2]

[1]The First School of Clinical Medicine, Lanzhou University, Lanzhou, Gansu Province, People's Republic of China; [2]Gansu Provincial Maternity and Child-Care Hospital (Gansu Provincial Center Hospital), Lanzhou, Gansu Province, People's Republic of China

*These authors contributed equally to this work

Correspondence: Jian Liu; Lei Zhang, Email medecinliujian@163.com; 15403876@qq.com

Background: Sepsis is a life-threatening condition characterized by organ dysfunction due to an impaired immune response to infection. The lungs are highly susceptible to infection, often resulting in acute lung injury (ALI). The immune-related GTPase M (IRGM) and its murine homolog Irgm1 mediate autophagy and are implicated in inflammatory diseases, yet their roles in sepsis-induced ALI remain unclear.

Methods: We used RNA sequencing and bioinformatics to explore IRGM regulation. Sepsis-induced ALI was modeled in mice using cecal ligation and puncture (CLP). An in vitro model was created by stimulating A549 cells with lipopolysaccharide (LPS).

Results: In A549 cells, LPS treatment induced upregulation of IRGM expression and enhanced autophagy levels. IRGM knockdown exacerbated LPS-induced ALI, characterized by suppressed autophagy and increased apoptosis, along with significantly elevated levels of p-AKT and p-mTOR. Further investigation revealed that treatment with the AKT inhibitor MK2206 effectively reversed the autophagy inhibition caused by IRGM knockdown and reduced apoptosis. These findings suggest that the AKT/mTOR signaling pathway plays a crucial role in IRGM-mediated protection against sepsis-related ALI.

Conclusion: This study identifies the protective role of IRGM in sepsis-induced ALI and reveals that IRGM mitigates ALI by promoting autophagy through inhibition of the AKT/mTOR pathway. These findings provide insights into the pathogenesis of sepsis-related ALI and highlight IRGM as a potential therapeutic target.

Keywords: sepsis-induced acute lung injury, IRGM, AKT/mTOR signaling pathway, autophagy

Introduction

Sepsis is a life-threatening condition resulting from an inappropriate host response to infection, often leading to organ dysfunction.[1] It is a major cause of death in intensive care units, with mortality rates ranging from 25% to 35%.[2,3] The early stage of sepsis is characterized by excessive immune activation,[4] followed by immune suppression, which compromises the host's ability to clear pathogens. The lungs, being one of the earliest and most vulnerable organs affected by sepsis, are commonly implicated in the development of ALI. ALI results from widespread damage to pulmonary capillary endothelial cells and alveolar epithelial cells, causing pulmonary edema, alveolar collapse, respiratory distress, and refractory hypoxemia.[5] Despite advances in mechanical ventilation and supportive therapies, mortality in patients with sepsis-associated ALI remains high, and clinical outcomes are poor.

The term "autophagy", originating from the Greek word for "self-eating", was first coined by Christian de Duve more than 40 years ago. Autophagy is a well-preserved catabolic mechanism that enables the breakdown and recycling of damaged organelles and macromolecules through lysosomal activity, thus preserving cellular homeostasis during adverse conditions.[6,7] However, the function of autophagy in sepsis-induced ALI remains a subject of debate. While some studies have reported protective effects,[8,9] others suggest that autophagy may exacerbate damage,[10,11] leading to conflicting

Received: 17 September 2024
Accepted: 23 November 2024
Published: 4 December 2024

conclusions. On the one hand, autophagy is induced as an essential adaptive response in various pathological conditions, including ischemia/reperfusion injury, hypoxia, sepsis-associated ALI, and inflammation, where it alleviates these processes.[12–14] This indicates that autophagy may be a potential therapeutic target for managing or reducing the progression of sepsis-induced ALI. Conversely, excessive autophagy can cause cell death, which can exacerbate lung damage in sepsis.[15] Therefore, further investigation is required to elucidate how autophagy regulates sepsis-induced ALI.

Immunity-related GTPase M (IRGM), a key member of the interferon-inducible GTPases (IRGs) family, is recognized as a potent intracellular pathogen defense molecule.[16] A landmark study demonstrated that murine Irgm1 and its human ortholog, IRGM, play a critical role in inducing autophagy and clearing intracellular Mycobacterium tuberculosis.[17] Subsequent research has shown that Irgm1-mediated autophagy also supports the survival of autoreactive T cells, ischemic neurons, and melanoma cells.[18–21] Moreover, IRGM is linked to the development of inflammatory bowel disease and plays a role in regulating autophagy. Studies have shown that under conditions of nutrient deprivation, bacterial, and viral infections, IRGM regulates autophagy by inactivating the mTOR signaling pathway.[22] As one of the core pathways regulating autophagy, inhibition of the AKT/mTOR signaling pathway has been shown to effectively activate autophagy and plays a crucial role in enhancing the immune response to bacterial invasion.[23,24] Despite its role in various inflammatory and autoimmune diseases, the specific role and mechanisms of IRGM in sepsis-induced ALI are still not well elucidated. Therefore, this study sought to explore the role of IRGM in sepsis-induced ALI.

This study aimed to clarify the impact of IRGM on autophagy and apoptosis in the context of sepsis-induced ALI. Furthermore, we explored how the AKT/mTOR signaling pathway influences autophagy regulated by IRGM. Our results highlight the essential role of IRGM in sepsis-related ALI and may identify new therapeutic targets for clinical treatment of sepsis-induced ALI.

Materials and Methods

Bioinformatic Analysis

Bioinformatics analysis was carried out on the datasets GSE2411, GSE18341, and GSE60088, which were sourced from the Gene Expression Omnibus (GEO) database (http://www.ncbi.nlm.nih.gov/geo/). The GSE2411 dataset comprised 6 control lung tissue samples and 6 sepsis-induced ALI samples. GSE18341 included 8 control lung tissue samples and 8 sepsis-induced ALI samples, while GSE60088 contained 4 control lung tissue samples and 5 sepsis-induced ALI samples.

Animals

Male C57BL/6J mice (6–8 weeks old, 20–24 g), maintained in a specific pathogen-free (SPF) environment, were obtained from the Experimental Animal Center of Lanzhou University. The animals were kept in a pathogen-free environment with controlled temperature (22±1°C) and humidity (60±10%). All experimental procedures followed the Animal Welfare Committee guidelines of the First Hospital of Lanzhou University and received approval from the Institutional Animal Care and Use Committee (LDYYLL2024-400).

Cecal Ligation and puncture (CLP) Surgery

A total of 24 C57BL/6J mice were randomly assigned to four groups, with six mice per group: Sham, CLP 6 hours, CLP 12 hours, and CLP 24 hours. The CLP procedure was carried out according to established protocols.[25] Mice were anesthetized using an intraperitoneal injection of 1% sodium pentobarbital at a dose of 50 mg/kg. After anesthesia, the mice were positioned on a surgical platform, and their abdominal fur was shaved. A 1 cm incision was made along the midline, and the abdominal cavity was opened layer by layer to access the cecum. A ligature was placed using 3/0 silk suture approximately one-third from the tip of the cecum. Following this, the cecum was punctured twice with a 21-gauge needle to release intestinal contents. After these procedures, the cecum was repositioned within the abdominal cavity, and the incision was closed in layers before final disinfection. Mice in the sham surgery group underwent the same procedure, with the exception that the cecum was not subjected to ligation or puncture. Following the CLP procedure, mice received subcutaneous injections of physiological saline (50 mL/kg) for fluid resuscitation. All animals

were euthanized by intraperitoneal injection of sodium pentobarbital (150 mg/kg), and tissue samples were subsequently collected for further experiments.

Hematoxylin and Eosin (H&E) Staining

The lower lobe of the left lung from each group of mice was collected and fixed in 4% paraformaldehyde for 24 hours. After dehydration through a series of graded ethanol and embedding in paraffin, 4 μm-thick tissue sections were sliced with a microtome. The specimens were then treated with H&E, dehydrated in ethanol, cleared with xylene, and mounted in neutral resin. Morphological alterations in lung tissues were examined under a microscope, and histopathological scoring of lung injury was performed according to the method described in reference.[26,27]

Immunohistochemical Staining

Paraffin-embedded tissue blocks were sliced into 5 μm sections and then processed for deparaffinization and rehydration. Subsequently, the sections were incubated in 3% H_2O_2 solution to inhibit endogenous peroxidase activity and subsequently incubated with goat serum for 30 minutes at ambient temperature. Subsequently, the samples were treated with Irgm1 antibody and incubated overnight at 4°C. The next day, after washing with PBS, the sections were exposed to the corresponding secondary antibody and incubated at room temperature for 1 hour. After a final PBS wash, the sections were developed using a DAB staining kit. The slides were then counterstained with hematoxylin, dehydrated, cleared, mounted in neutral resin, and examined under a light microscope.

Enzyme-linked Immunosorbent Assay (ELISA)

Tumor necrosis factor-α (TNF-α) and interleukin-1β (IL-1β) levels in mouse serum were assessed using ELISA kits from Dakewe Biotech Co., Ltd. (Shenzhen, China) following the manufacturer's guidelines.

Lung Wet-to-Dry (W/D) Weight Ratio Assay

Mice were euthanized at 6, 12, and 24 hours post-CLP, and the left lung was promptly excised. Lung tissue was first weighed to determine its wet weight. It was then placed in a drying oven at 80°C for 48 hours to remove moisture, after which the dry weight was measured.

Bronchoalveolar Lavage Fluid (BALF)

Three milliliters of PBS were introduced into the trachea, and the lungs were softly washed three times to gather BALF. The fluid was centrifuged at 350 g for 5 minutes at 4°C to separate the supernatant, which was then analyzed for protein content using a bicinchoninic acid (BCA) assay.

Cell Culture and treatment

A549 cells were obtained from Wuhan Zishan Biotechnology Co., Ltd. and cultured in DMEM medium supplemented with 10% fetal bovine serum (FBS; Gibco, USA) in a 5% CO2 humidified incubator at 37°C. To create an in vitro model of sepsis-associated ALI, A549 cells were exposed to lipopolysaccharide (LPS; Sigma, USA) to induce cellular damage. The lentivirus for IRGM gene knockdown (sh-IRGM) and the control (sh-NC) were provided by GeneChem Co., Ltd. (Shanghai, China). Transfections were executed per the manufacturer's protocol, and efficiency was measured 72 hours later. Subsequently, the cells were exposed to 20 μg/mL LPS for 24 hours, or pre-treated with the AKT inhibitor MK2206 (50 μM) for 24 hours prior to LPS exposure, and then harvested for molecular analysis.

Cck-8

A549 cells were seeded into 96-well plates at a rate of 5×10^3 cells per individual well. After 48 hours, CCK-8 reagent (Solarbio, Beijing, China, CA1210) was added at 10 μL per 100 μL of medium and incubated at 37°C for 2 hours. The optical density (OD) was measured at 450 nm. Cell viability was evaluated based on absorbance values compared to a standard curve. Each experiment was performed in triplicate.

EdU Assay

Cell proliferation was assessed using the BeyoClick™ EdU Cell Proliferation Detection Kit (Beyotime, Shanghai, China, C0075). A549 cells were initially grown in 6-well plates using DMEM medium with 10% serum. The cells were then incubated with EdU-containing medium for 2 hours. Following the removal of the EdU-containing medium, the cells were rinsed with PBS and then fixed with formaldehyde to preserve the incorporated EdU. Following fixation, the cell membranes were permeabilized using an appropriate permeabilization buffer. The cells were incubated with the click chemistry reaction mixture containing the fluorescent probe for 30 minutes. Following incubation, the cells were rinsed with a suitable buffer to remove excess reagents. Subsequently, fluorescence microscopy was used to analyze the cells.

Western Blot Analysis

Proteins from A549 cells or lung tissue samples were isolated using RIPA lysis buffer containing protease and phosphatase inhibitors. Protein levels were determined with a BCA assay kit. The proteins were then resolved by SDS-PAGE and transferred to PVDF membranes. After blocking with 5% non-fat milk for 1 hour at room temperature, the membranes were incubated overnight at 4°C with specific primary antibodies. The primary antibodies used are as follows: IRGM (1:1000, NBP1-76377, Novus), Irgm1 (1:1000, MA9427, Abmart), LC3 (1:1000, #3868, CST), p62 (1:2000, 18,420-1-AP, Proteintech), Beclin1 (1:2000, 11,306-1-AP, Proteintech), Bax (1:3000, 50,599-2-Ig, Proteintech), Bcl2 (1:2000, ab12858, abcame), Caspase9 (1:1000, 10,380-1-AP, Proteintech), AKT (1:2000, 10,176-2-AP; Proteintech), p-AKT (1:1000, #9271, CST), mTOR (1:1000, 66,888-1-Ig, Proteintech), p-mTOR (1:1000, #5536, CST), β-actin (1:1000, #4967, CST). Following this, the membranes were treated with the relevant secondary antibody at room temperature for 1 hour. The target proteins were then detected using a chemiluminescence reagent and visualized with a chemiluminescence imaging system. The intensity of the target bands was quantified with ImageJ software, using β-actin levels as an internal control for normalization.

Quantitative Real-time Polymerase Chain Reaction (qRT-PCR)

RNA was isolated from cells using the RNA extraction kit (NCM, Suzhou, China). The total RNA was then converted into cDNA. Gene expression was quantified through qRT-PCR with Power SYBR Green PCR Master Mix (Takara, Shiga, Japan). GAPDH levels served as an internal control to normalize the expression of target genes. The primers of target genes were: IRGM-Forward, CGAAACACAGGACATGAGGGTAAG; IRGM-Reverse, GAAATAGGAGGCACATCTTTGGGTAG.

RNA Sequencing

A549 cells transfected with sh-IRGM and sh-NC were collected after 24 hours of LPS treatment and subjected to RNA sequencing (RNA-seq) by OE Biotech Co., Ltd. (China) following standard protocols. Differentially expressed genes were identified with thresholds of $P<0.05$ and FDR$\leq$0.25. Key genes were then analyzed for their involvement in pathways using KEGG analysis through OECloud tools (https://cloud.oebiotech.com).

Autophagy Flux Analysis

A549 cells were cultured in confocal dishes and reached 50–60% confluency at the time of infection. The cells were then transduced with Ad-mRFP-GFP-LC3B adenovirus (GeneChem, Shanghai, China) at a multiplicity of infection (MOI) of 10 for 24 hours. After the transduction period, the adenovirus-containing medium was removed. The infected cells were subjected to various stimuli and treated for an additional 24 hours. Autophagic flux was visualized using a confocal microscope (Zeiss, Germany) and evaluated by counting the yellow and red fluorescent spots.

Flow Cytometry

Apoptosis was assessed using an apoptosis detection kit (Elabscience, Wuhan, China). Cells from each group were resuspended in 500 μL of 1× Annexin V Binding Buffer to create a single-cell suspension. Subsequently, 5 μL of Annexin V-FITC and 5 μL of PI were added, and the mixture was gently mixed and incubated in the dark at room temperature for 15 minutes. Apoptosis was then assessed within 1 hour using a flow cytometer.

Immunofluorescence

Cell samples were initially fixed in 4% paraformaldehyde at room temperature for 15 minutes to preserve cellular integrity. Next, cells were permeabilized using 0.1% Triton X-100 for 5–10 minutes and then blocked with 5% bovine serum albumin (BSA) for 30 minutes to reduce nonspecific binding. Following this, the samples were incubated overnight at 4°C with primary antibodies. The primary antibodies used were as follows: p-AKT (1:1000, #9271, CST), p-mTOR (1:1000, #5536, CST), LC3 (1:1000, #3868, CST), and Caspase9 (1:1000, 10,380-1-AP, Proteintech). After washing, a secondary antibody conjugated to a fluorescent dye was applied for 1 hour at room temperature in the dark. Finally, the samples were mounted with DAPI for nuclear visualization and analyzed with a fluorescence microscope.

Statistical Analyses

Statistical analyses and graphical representations were conducted using GraphPad Prism 9 software. Experimental data are presented as mean±SD from at least three independent trials. Group differences were evaluated with one-way ANOVA or an unpaired *t*-test, with significance defined as a p-value of <0.05.

Results

DEGs in Sepsis-Induced ALI Were Identified Through a Combined Analysis of Multiple Microarray Datasets

To explore the molecular mechanisms of ALI, we analyzed three datasets (GSE2411, GSE18341, and GSE60088) from the GEO database to identify differentially expressed genes (DEGs) in a murine model of sepsis-induced ALI. Heatmap and volcano plot analyses of these datasets (Figure 1A-C) revealed the expression profiles of the DEGs. Venn diagram analysis identified 23 commonly upregulated DEGs across the three datasets (Figure 1D). The 23 identified DEGs were subsequently analyzed using the STRING database to construct a PPI network (Figure 1E). Using six topological analysis methods provided by the CytoHubba plugin, we ranked the nodes in the PPI network, revealing Irgm1, Gbp2, and Gbp3 as key hub genes (Figure 1F). Given the novelty and existing literature, we noted that there is relatively limited research on Irgm1 in the context of sepsis-induced ALI, prompting us to focus on this gene for further investigation. In all three GEO datasets, Irgm1 was significantly upregulated in ALI samples (Figure 1G). Based on these findings, we selected Irgm1 as a key gene for subsequent studies.

In Mice with Sepsis-Induced ALI, Irgm1 Expression Increases Concomitantly with the Activation of Autophagy

To investigate the role of Irgm1 in autophagy regulation, we established a murine sepsis-induced ALI model using the CLP method and conducted observations at 6, 12, and 24 hours post-operation. At the 12-hour mark, serum levels of IL-1β and TNF-α showed a significant rise, which persisted through 24 hours (Figure 2A-B). Simultaneously, the lung W/D weight ratio and protein content in BALF increased at 12 hours, reaching their highest levels by 24 hours (Figure 2C-D). To further validate the successful induction of the ALI model, we performed H&E staining on lung tissues from each group, followed by histopathological analysis (Figure 2E-F). The sham-operated group exhibited normal cellular morphology and arrangement. In contrast, the 24-hour CLP group showed marked histopathological changes in the lung tissue, including interstitial congestion and edema, thickening of the alveolar walls, and extensive infiltration of inflammatory cells into the alveolar spaces. These results indicate that we successfully established a murine model of sepsis-induced ALI.

To further investigate the potential role of autophagy in sepsis-induced ALI, we assessed the expression of LC3, p62, and Beclin1 by Western blotting (Figure 2G). The results revealed a significant increase in the levels of the autophagy markers LC3-II /LC3-I and Beclin1 at 12 hours, with a peak at 24 hours. In contrast, p62 levels showed a marked decrease as early as 6 hours. Additionally, the protein expression level of Irgm1 gradually increased at 12 and 24 hours post-CLP, demonstrating a time-dependent upregulation. To further confirm the expression changes of Irgm1, we employed immunohistochemistry to evaluate Irgm1 protein levels in lung tissues from each group. The results indicated

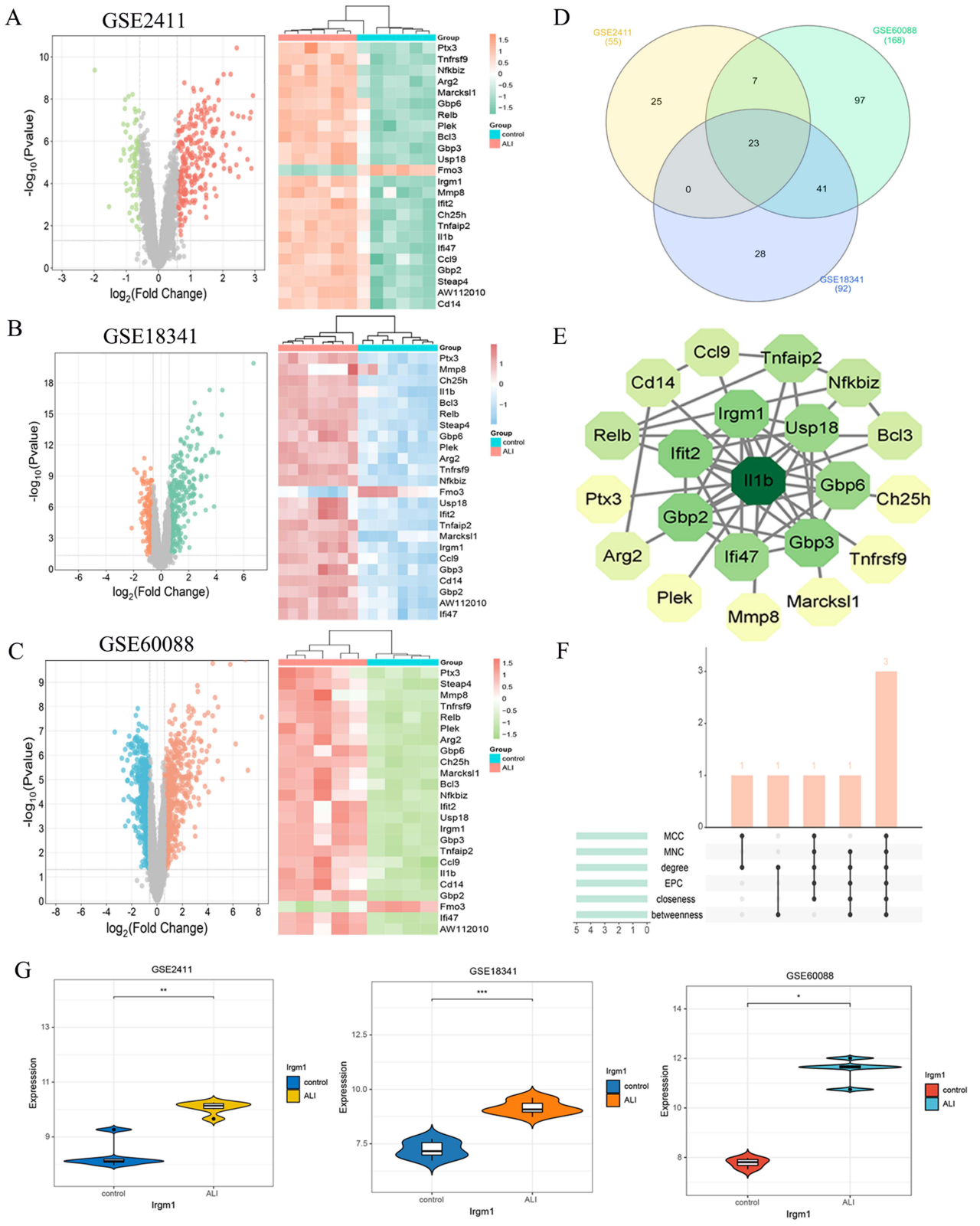

Figure 1 Identification of DEGs in ALI by multi-microarray combined analysis. (**A**) Volcano plot and heat maps of DEGs in GSE2411 database; (**B**) Volcano plot and heat maps of DEGs in GSE18341 database; (**C**) Volcano plot and heat maps of DEGs in GSE60088 database; (**D**) Venn diagram of up-regulated DEGs based on three GEO datasets; (**E**) PPI network of DEGs; (**F**) CytoHubba plugin identified three hub genes; (**G**) The expression of Irgm1 gene in GSE2411, GSE60088, and GSE18341 GEO datasets.

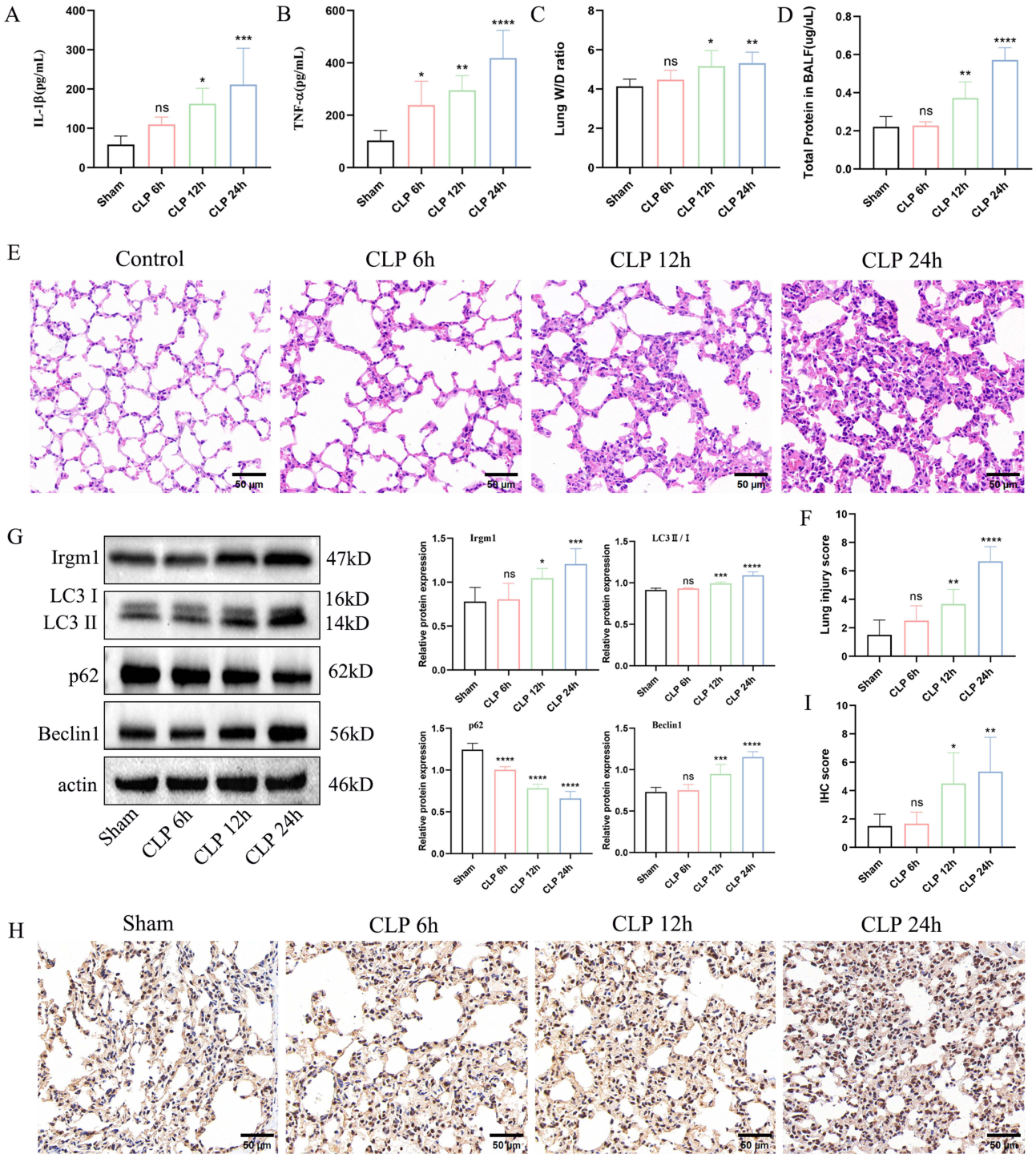

Figure 2 Expression of Irgm1 in the CLP-induced ALI mouse model. (**A-B**) ELISA was used to test the concentration of IL-1β and TNF-α in serum (n=6); (**C**) Lung wet/dry (W/D) ratio (n=6); (**D**) Total cell protein concentrations (n=6); (**E**) HE staining was used to detect lung tissue morphology. Scale bars: 50 um; (**F**) The lung injury score was assessed using histological sections (n=6); (**G**) Expression of Irgm1 and autophagy-associated proteins in the lung tissues of the CLP-induced ALI mouse model (n=3); (**H-I**) Immunohistochemical staining to analyze the expression and distribution of Irgm1 in the lung tissues of CLP-induced ALI mouse model (n=6). Scale bars: 50 um. Data are presented as mean±SD values, **P* < 0.05,** *P* < 0.01, ****P* < 0.001, *****P* < 0.0001 versus Sham.

a significant upregulation of Irgm1 in lung tissues at 24 hours post-CLP (Figure 2H-I). These findings suggest that Irgm1, along with autophagy-related proteins, is upregulated in response to CLP-induced ALI, indicating a potential involvement of Irgm1 in the autophagic process associated with sepsis-induced ALI.

IRGM Knockdown Increases LPS-Induced Death in A549 Cells

Since autophagy plays a key regulatory role in lung injury, the expression levels of IRGM and autophagy markers (LC3II/I, p62 and Beclin1) were examined by Western blot. The results demonstrated a clear concentration- and time-dependent response. In the concentration gradient experiment, increasing LPS concentrations led to a significant elevation in the levels of IRGM and autophagy markers (LC3II/I and Beclin1), particularly at 20 μg/mL, with a subsequent slight decrease. Conversely, p62 expression was markedly reduced and then slightly rebounded (Figure 3A and C). Based on these findings, we selected 20 μg/mL LPS for treatment of A549 cells for 12, 24, and 48 hours. The results showed that the expression levels of IRGM and autophagy markers (LC3II/I and Beclin1) peaked at 24 hours before slightly declining, while p62 expression reached its lowest point at 24 hours and then slightly increased (Figure 3B and D). Therefore, we determined that 20 μg/mL LPS and a 24-hour stimulation period were optimal conditions for subsequent in vitro experiments.

To further elucidate the mechanism by which IRGM modulates lung epithelial cell activity in sepsis-induced ALI, we first established a sepsis-induced ALI cell model using LPS-treated A549 cells. Following this, IRGM expression was silenced, and the knockdown efficiency was confirmed through qRT-PCR and Western blot assays. Results demonstrated that sh-IRGM#1 exhibited higher efficiency in IRGM gene knockdown compared to sh-IRGM#2. Therefore, sh-IRGM#1 was selected for use in subsequent experiments (Figure 4A-C). To assess the effects of IRGM knockdown on cell

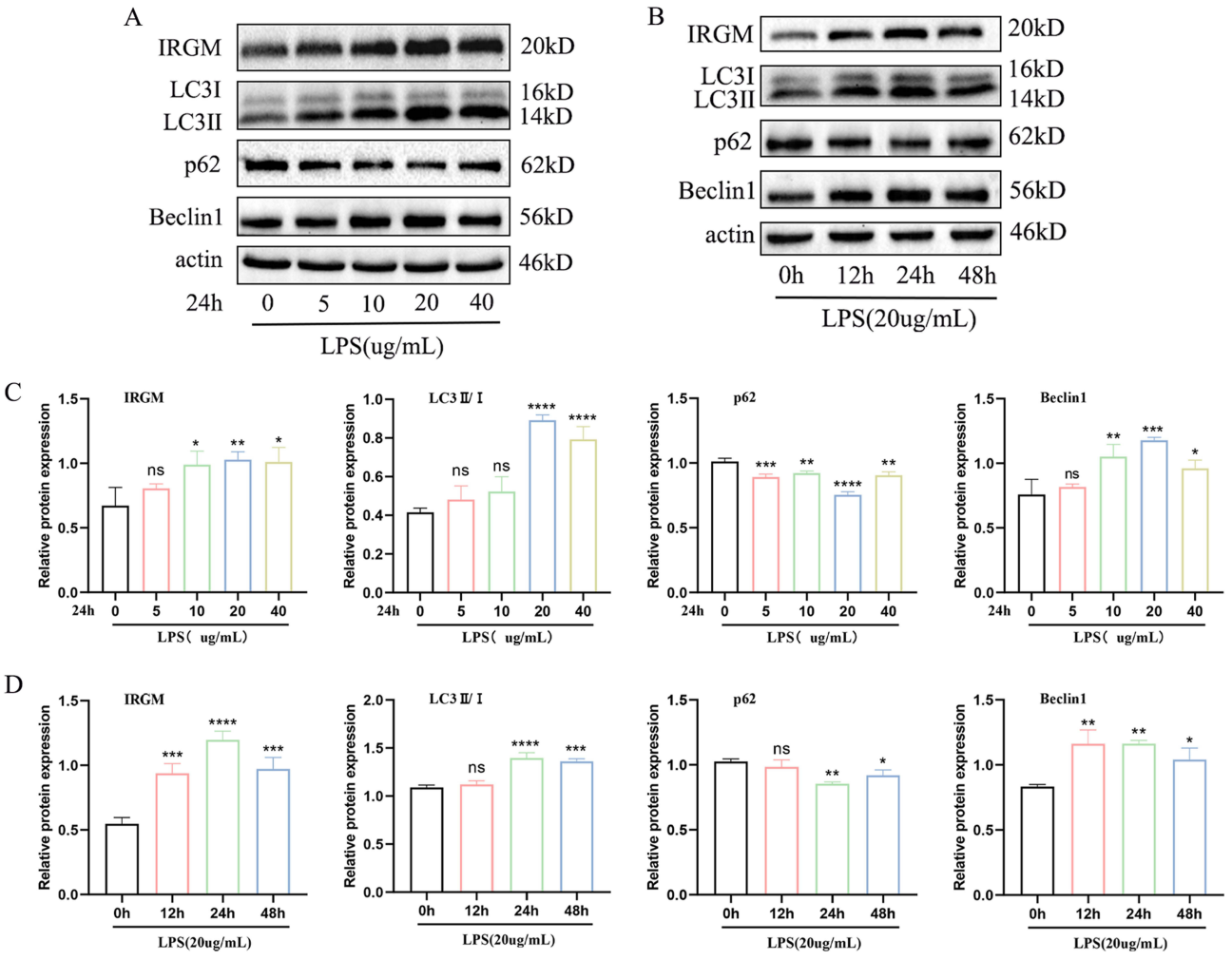

Figure 3 The effect of LPS in A549 cells. (**A,C**) Expression of IRGM, LC3, p62, and Beclin1 were determined using Western blotting with LPS at different concentrations; (**B,D**) Expression of IRGM, LC3, p62, and Beclin1 were determined using Western blotting with LPS at different times. Each experiment is repeated three times, and the data are presented as mean ± SD values, *$P < 0.05$,** $P < 0.01$, ***$P < 0.001$, ****$P < 0.0001$ versus Sham.

viability, we evaluated cell growth with CCK-8 and EdU assays. Our analysis indicated that LPS treatment significantly diminished the viability of A549 cells. Following IRGM knockdown, the LPS-induced suppression of cell viability was further exacerbated (Figure 4D-F). These findings suggest that IRGM may mitigate the progression of ALI by preserving lung epithelial cell activity.

IRGM Regulates the AKT/mTOR Signaling Pathway and Autophagy

To investigate the mechanism by which IRGM alleviates sepsis-induced ALI, we developed a cell line with stable IRGM knockdown (sh-IRGM). Subsequently, we performed transcriptome sequencing analysis on LPS-stimulated sh-IRGM cells (LPS+sh-IRGM) and their corresponding negative controls (LPS+sh-NC) (Figure 4G). Data analysis revealed that IRGM knockdown resulted in significant expression changes in 1913 genes (log2 FC > 1) (Figure 4H). To further elucidate the downstream molecular mechanisms regulated by IRGM, we conducted KEGG pathway enrichment analysis on the DEGs, identifying the top 20 most significantly enriched signaling pathways. The results indicated that the PI3K-AKT and TNF signaling pathways were highly enriched among the DEGs (Figure 4I). Notably, earlier studies have identified the PI3K-AKT signaling pathway as pivotal in modulating autophagy,[28] which is considered an important regulatory mechanism in the progression of LPS-induced sepsis ALI.

To assess the impact of IRGM knockdown on the autophagic process in LPS-induced ALI, we evaluated the protein expression levels of autophagy markers LC3 II/II, Beclin-1, and p62 using Western blot. The results demonstrated a significant increase in LC3 II/I and Beclin-1 expression levels following LPS induction, alongside a marked decrease in p62 levels. In contrast, IRGM knockdown significantly inhibited the LPS-induced upregulation of LC3 II/I and Beclin-1, while concurrently elevating p62 expression (Figure 5A). Additionally, we employed the mRFP-GFP-LC3 adenovirus vector to monitor autophagic flux.[29] The findings revealed that LPS stimulation led to a substantial increase in autophagic flux. However, IRGM gene silencing markedly attenuated the LPS-induced increase in autophagic flux (Figure 5B-D). To further elucidate the involvement of the AKT/mTOR signaling axis in the regulation of autophagy by IRGM, we analyzed the expression levels of AKT, p-AKT, mTOR, and p-mTOR using Western blot. The results showed a significant reduction in p-AKT/AKT and p-mTOR/mTOR protein levels following LPS stimulation. Notably, IRGM knockdown led to a significant upregulation in the ratio of p-AKT to AKT and p-mTOR to mTOR protein levels (Figure 5E). Collectively, these findings suggest that IRGM may enhance the autophagic process by inhibiting the AKT/mTOR signaling pathway, thereby providing protective effects on A549 cells and alleviating sepsis-induced ALI.

IRGM Knockdown Exacerbates Apoptosis in LPS-Induced ALI

To elucidate IRGM's impact on cell apoptosis, we assessed the abundance of various apoptosis-related markers using Western blot analysis. The results indicated that IRGM knockdown significantly enhanced the upregulation of pro-apoptotic proteins Bax, and cleaved-caspase9 in LPS-treated A549 cells, while further suppressing the levels of the Bcl2 (Figure 6A). To further validate the impact of IRGM on cell apoptosis, we performed quantitative analysis of apoptosis rates using flow cytometry. The results demonstrated that LPS significantly increased the apoptosis rate, and down-regulation of IRGM further exacerbated LPS-induced apoptosis (Figure 6B). These findings are consistent with the Western blot results and further confirm the protective role of IRGM in regulating LPS-induced apoptosis.

AKT/mTOR Signaling Pathway Inhibitors Specifically Reverse the Impact of IRGM Deficiency on LPS-Induced ALI

To further elucidate the mechanism by which the AKT/mTOR signaling pathway mediates IRGM regulation of autophagy, we conducted intervention experiments using the specific AKT inhibitor MK2206 (50 μM). Western blot and immunofluorescence analyses were employed to assess the expression levels of AKT, p-AKT, mTOR, and p-mTOR. The results demonstrated that MK2206 treatment markedly decreased the ratios of p-AKT to AKT and p-mTOR to mTOR relative to those observed in the LPS+sh-IRGM group (Figure 7A-E). Subsequently, we evaluated the abundance of LC3 II/I, Beclin-1, and p62 by Western blot, and further confirmed LC3 expression and distribution through immunofluorescence staining. MK2206 treatment was found to significantly upregulate LC3 II/I and Beclin-1 expression

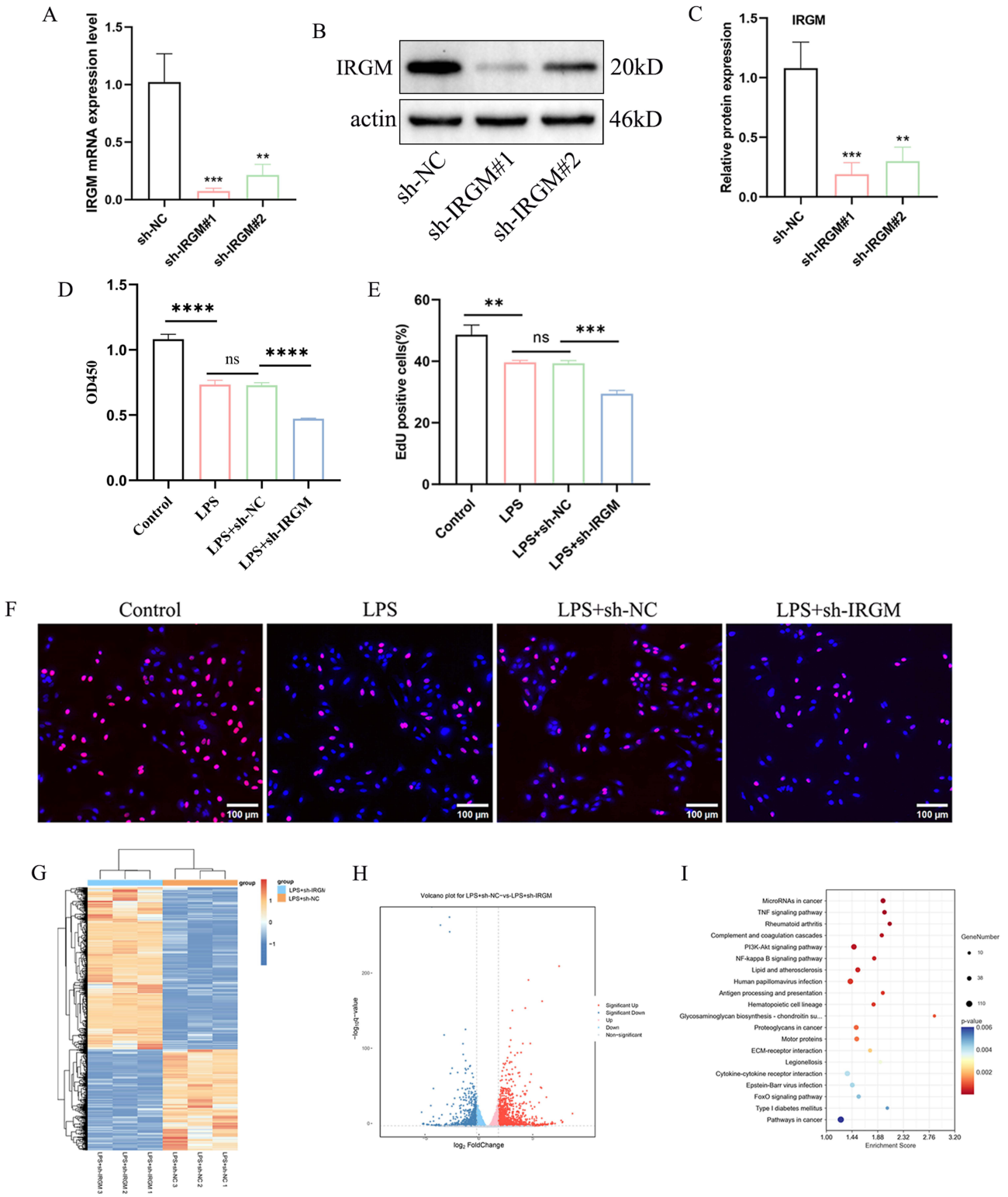

Figure 4 IRGM knockdown inhibited LPS-induced A549 cell viability. (**A-C**) qRT-PCR and Western blot analysis were performed to detect the mRNA and protein expression levels of IRGM after IRGM knockdown; (**D-F**) CCK-8 and EdU staining were used to analyze the growth activity of A549 cells; (**G**) The hierarchical clustering heat maps of DEGs for LPS+sh-IRGM vs LPS+sh-NC (n=3). The more purple it is, the higher the expression level; the bluer it is, the lower the expression level; (**H**) DEGs volcano map of LPS+sh-IRGM vs LPS+sh-NC; (**I**) KEGG enrichment analysis for DEGs of LPS+sh-IRGM vs LPS+sh-NC. Scale bars: 100 um. Each experiment is repeated three times, and the data are presented as mean ± SD values, $^{**}P < 0.01$, $^{***}P < 0.001$, $^{****}P < 0.0001$ versus Sham.

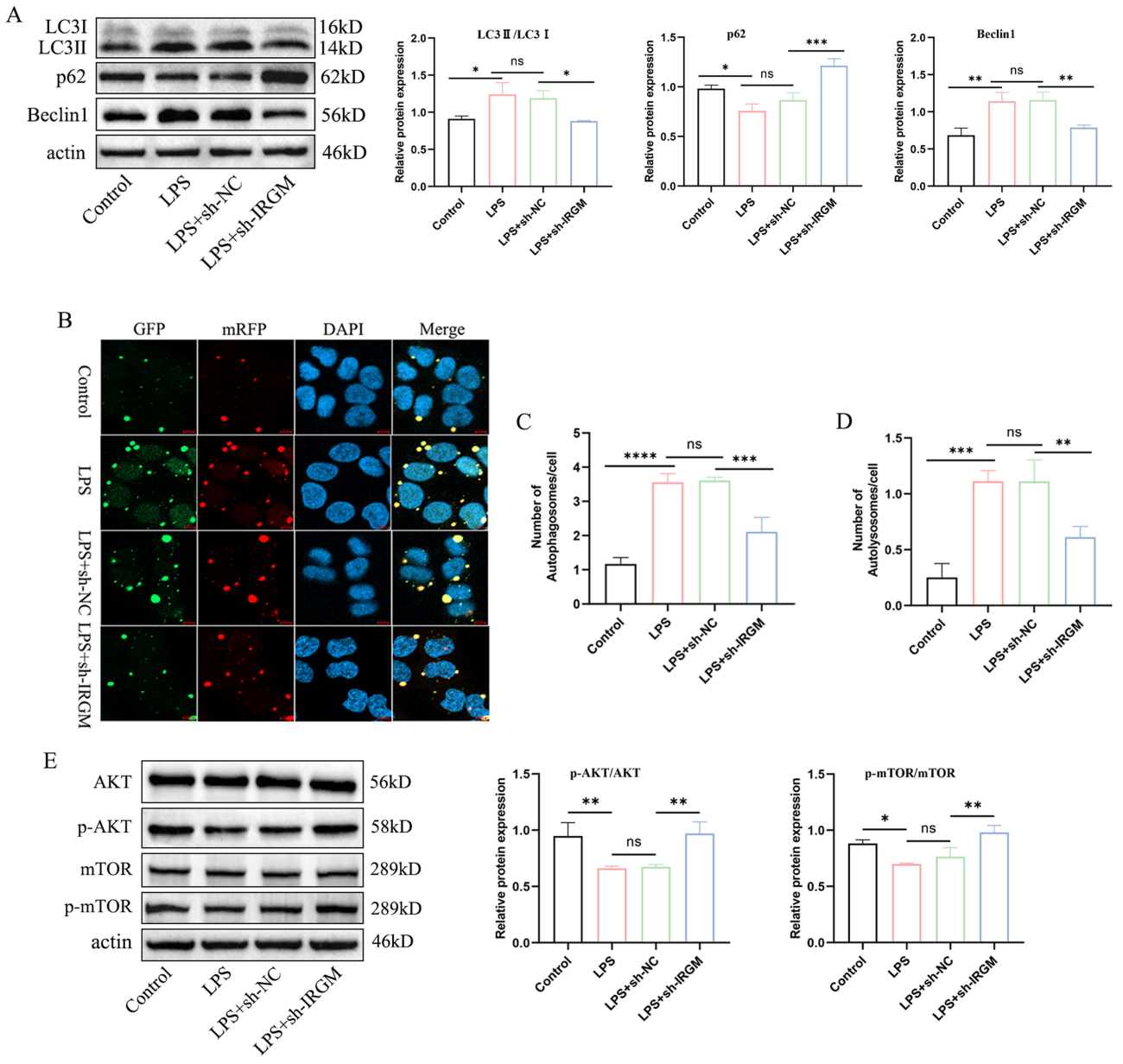

Figure 5 IRGM-regulated AKT/mTOR signaling pathway and autophagy. (**A**) Levels of autophagy-related proteins were evaluated by Western blot; (**B**) Figure B displays representative confocal images of admCherry-GFP-LC3 cells. The GFP and mRFP fluorescent signals were used to detect autophagosomes (yellow dots) and autolysosomes (red dots). Scale bars: 4 um; (**C-D**) Quantification of autophagosomes and autolysosomes; (**E**) The levels of AKT, p-AKT, mTOR, and p-mTOR were evaluated by Western blot. Each experiment is repeated three times, and the data are presented as mean ± SD values, *P < 0.05,** P < 0.01, ***P < 0.001, ****P < 0.0001 versus Sham.

while downregulating p62 expression, in contrast to the LPS+sh-IRGM group (Figure 8A-D). Moreover, the immunofluorescence staining of LC3 corroborated the Western blot results (Figure 8E-F). These findings highlight the pivotal role of the AKT/mTOR signaling pathway in the regulation of autophagy by IRGM.

Treatment with MK2206 in A549 cells significantly reversed the effects of IRGM knockdown, reversing the increase in pro-apoptotic proteins (Bax and cleaved-caspase9) and the decrease in the anti-apoptotic protein Bcl2 induced by LPS (Figure 9A-D). Flow cytometry analysis further confirmed that MK2206 significantly reduced the apoptosis rate associated with IRGM knockdown (Figure 9E and G). Additionally, immunofluorescence staining for cleaved-caspase9 supported these findings (Figure 9F and H). These results indicate that IRGM mitigates LPS-induced apoptosis in A549 cells by inhibiting the AKT/mTOR signaling pathway and promoting autophagy. This mechanism provides new

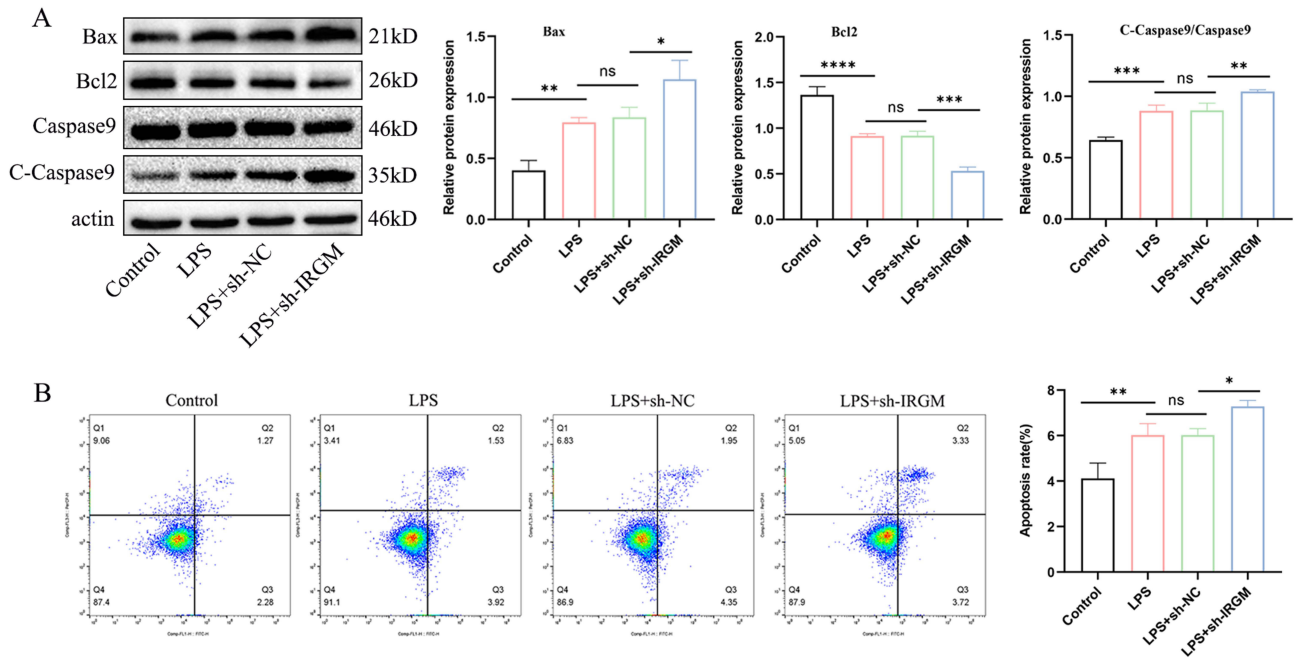

Figure 6 IRGM knockdown aggravated LPS-inducedA549 cell apoptosis. (**A**) Levels of apoptotic markers were evaluated by Western blot; (**B**) Apoptosis rate was detected using flow cytometry. Each experiment is repeated three times, and the data are presented as mean ± SD values, *$P < 0.05$,** $P < 0.01$, ***$P < 0.001$, ****$P < 0.0001$ versus Sham.

molecular insights into the protective role of IRGM in ALI and lays a theoretical foundation for developing therapeutic strategies targeting IRGM and the AKT/mTOR signaling pathway.

Discussion

ALI is a common complication of sepsis; however, effective therapeutic interventions remain limited.[30] To elucidate the molecular mechanisms underlying sepsis-induced ALI, we performed bioinformatics analyses on lung tissue samples from sepsis-induced ALI mice and normal controls, utilizing microarray datasets GSE2411, GSE18341, and GSE60088. Our findings identified Irgm1 as a key gene associated with sepsis-induced ALI.

In a normal physiological state, Irgm1 levels are relatively low, however, it is significantly upregulated in response to pathogen invasion.[31] In this study, a sepsis-induced ALI mouse model was established using the CLP method. The results showed high expression of Irgm1 in ALI samples, consistent with bioinformatics predictions. Importantly, Irgm1 expression levels were found to increase with autophagy activation, aligning with previous findings. In a permanent middle cerebral artery occlusion (pMCAO) mouse model, Irgm1 was upregulated on the ischemic side of the brain, accompanied by a pronounced autophagic response. Conversely, Irgm1 knockout mice exhibited nearly complete loss of neuronal autophagy function and a significant increase in infarct volume.[20] To further investigate the critical role of Irgm1 in autophagy regulation, we stimulated human lung epithelial A549 cells with 20 μg/mL LPS for 24 hours to establish an in vitro model of sepsis-induced ALI. Transcriptomic analysis was performed using RNA-seq technology. Comparison of transcriptomic data between LPS+sh-IRGM and LPS+sh-NC groups revealed that DEGs were mainly concentrated in the PI3K-AKT and TNF signaling pathways. Existing research indicates that the PI3K-AKT signaling pathway plays a crucial role in autophagy regulation.[32] Building on these results, we focused on the AKT/mTOR signaling axis for further investigation.

Autophagy is a process that maintains cellular homeostasis by degrading intracellular macromolecules. This mechanism not only provides essential resources to the cell but also sequesters and eliminates intracellular toxins, pathogens, and damaged cytoplasmic components, thereby preventing further cellular injury.[6,33] During autophagy, cytoplasmic LC3-I is converted into LC3-II on the autophagosomal membrane, marking the formation of autophagosomes.[34] p62 is a protein degraded during autophagy, and its degradation serves as an indicator of autophagosome formation.[35] Beclin1 is a crucial

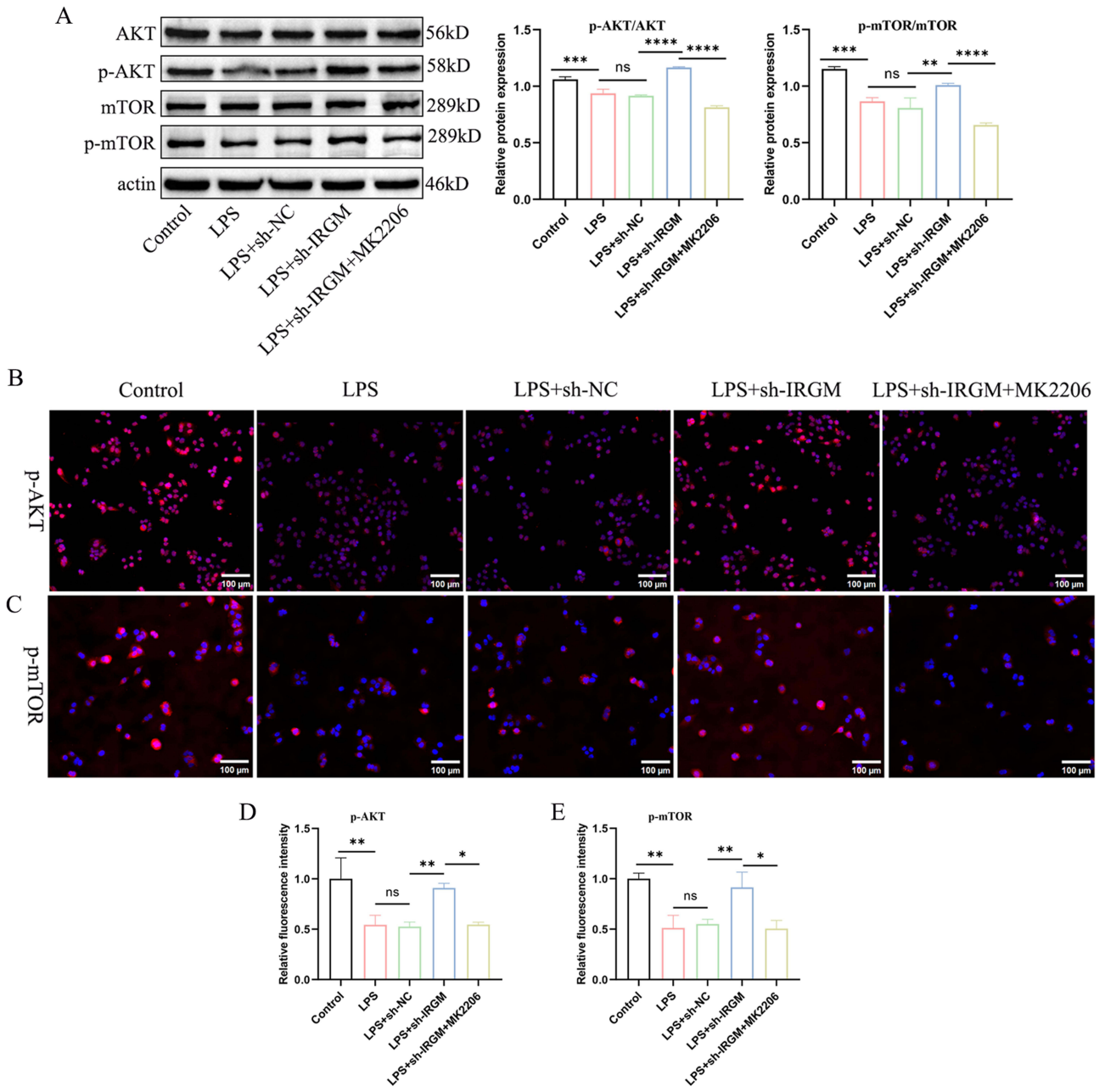

Figure 7 Inhibition of the AKT/mTOR signaling pathway partially reversed the activation of IRGM knockdown onAKT/mTOR pathway in LPS-inducedALI. (**A**) The levels of AKT, p-AKT, mTOR, and p-mTOR were evaluated by Western blot; (**B-E**) Immunofluorescence staining was used to detect the fluorescence intensity of p-AKT and p-mTOR in A549 cells. Scale bars: 100 um. Each experiment is repeated three times, and the data are presented as mean ± SD values, **P* < 0.05,** *P* < 0.01, ****P* < 0.001, *****P* < 0.0001 versus Sham.

regulatory protein in autophagy, playing a central role in the initiation of autophagy and the formation of autophagosomes.[36] Recent investigations underscore the essential role of autophagy activation in protecting against sepsis-induced ALI.[12,37] In a murine model of sepsis-induced ALI, silencing GGPPS1 diminished NLRP3 inflammasome activity and cell apoptosis by enhancing autophagy. However, this protective effect was abolished by the autophagy inhibitor 3-MA.[38] Our study found that LPS treatment significantly increased the LC3-II /I ratio and Beclin1 expression levels while decreasing p62 expression. Concurrently, mRFP-GFP-LC3 autophagy reporter assays indicated an increase in the number of autophagosomes. Conversely, IRGM knockdown impaired autophagy, leading to a significant reduction in A549 cell viability and an increase in cell apoptosis. This was accompanied by elevated levels of p-AKT and p-mTOR.

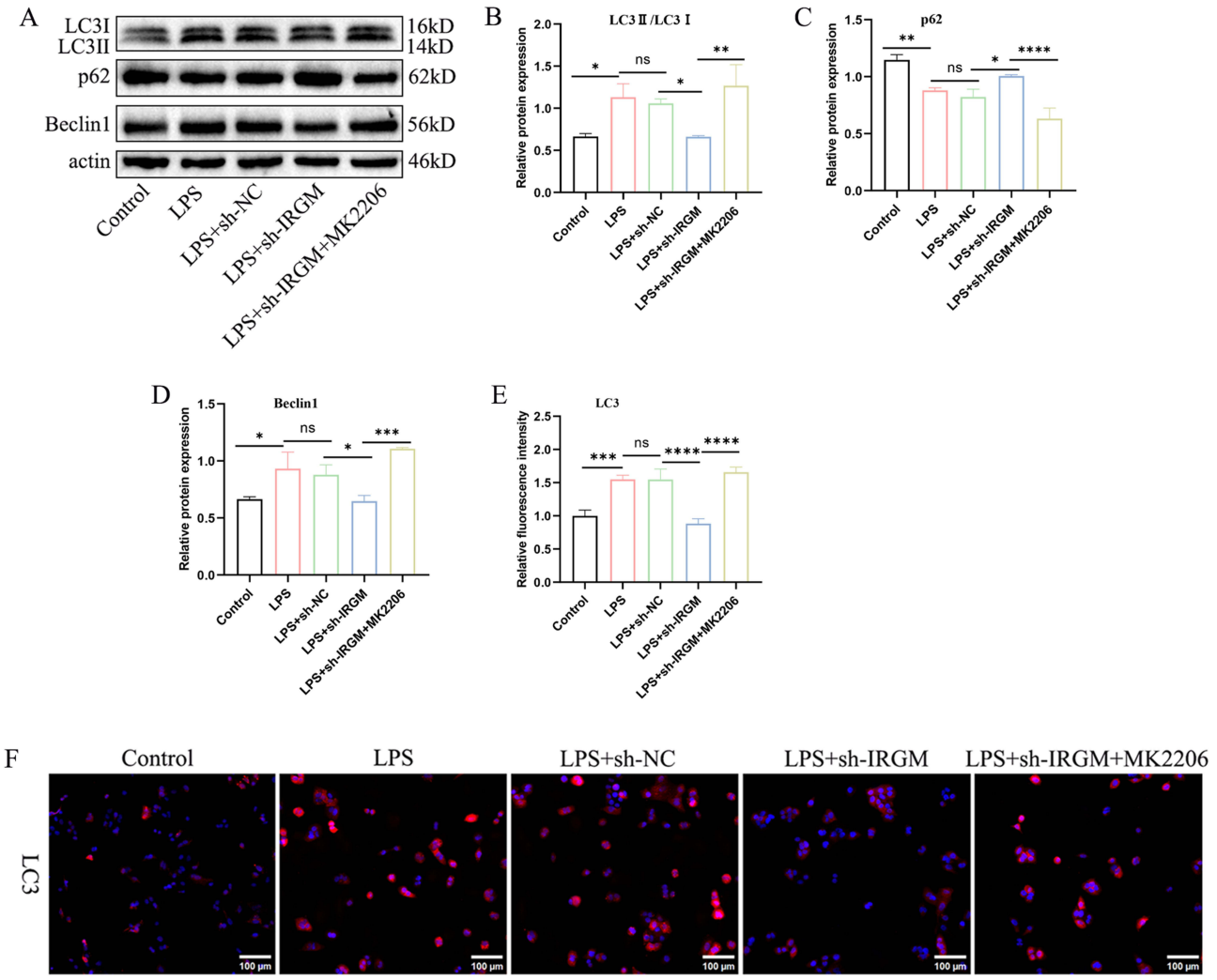

Figure 8 Inhibition of the AKT/mTOR signaling pathway partially reversed the inhibition of IRGM knockdown on autophagy in LPS-inducedALI. (**A-E**) Levels of autophagy-related proteins were evaluated by Western blot; (**F**) Immunofluorescence staining was used to detect the fluorescence intensity of LC3 in A549 cells. Scale bars: 100 um. Each experiment is repeated three times, and the data are presented as mean ± SD values, **P* < 0.05,** *P* < 0.01, ****P* < 0.001, *****P* < 0.0001 versus Sham.

These findings indicate that IRGM's protective role in sepsis-induced ALI may involve modulating autophagy through the AKT/mTOR signaling pathway.

The AKT/mTOR signaling pathway orchestrates a wide array of essential cellular processes, including cell proliferation, differentiation, migration, and survival, while also playing a pivotal role in the regulation of autophagic and apoptotic signaling.[31] Although mTOR is recognized as the primary regulator of autophagy, AKT activation suppresses autophagy through multiple mechanisms in cells.[39–41] AKT specifically phosphorylates and blocks the TSC1/2 complex, which activates RHEB GTPase. This, in turn, stimulates mTORC1 activity and suppresses autophagy.[42,43] Moreover, the AKT/mTOR signaling pathway is intricately involved in the regulation of both autophagy and apoptosis. AKT also phosphorylates the Bcl-2-associated death promoter (Bad), an anti-apoptotic molecule, which facilitates the release of the activated form of Bcl-2, preventing cytochrome c release and thereby halting the initiation of the apoptotic cascade.[44] While AKT activation temporarily inhibits apoptosis, the suppression of autophagy leads to the accumulation of cellular damage, which may eventually result in increased apoptosis. Multiple studies have demonstrated that enhancing autophagy through the modulation of the AKT/mTOR signaling pathway effectively mitigates sepsis-induced ALI. Qu et al demonstrated that glycyrrhizic acid significantly alleviates LPS-induced lung injury by inhibiting the PI3K-AKT-mTOR pathway, downregulating mTOR, and activating autophagy, thereby decreasing the secretion of inflammatory

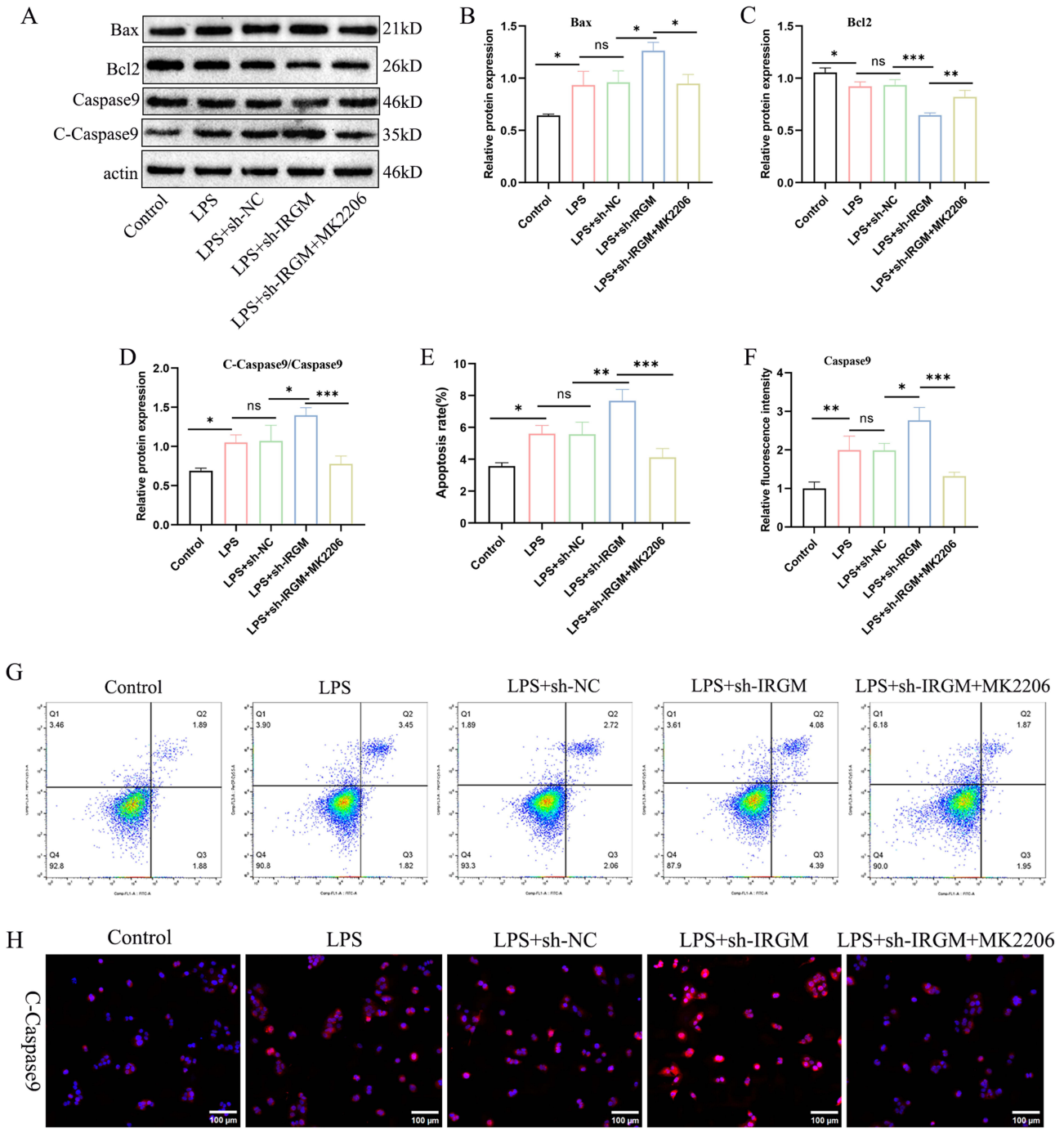

Figure 9 Inhibition of the AKT/mTOR signaling pathway partially reversed the activation of IRGM knockdown on autophagy in LPS-induced ALI. (**A-E**) Levels of apoptotic markers were evaluated by Western blot; (**F-G**) Apoptosis rate was detected using flow cytometry; (**H**) Immunofluorescence staining was used to detect the fluorescence intensity of cleaved-caspase9 in A549 cells. Scale bars: 100 um. Each experiment is repeated three times, and the data are presented as mean ± SD values, *$P < 0.05$,** $P < 0.01$, ***$P < 0.001$.

mediators and the generation of HMGB1.[45] Similarly, Zhang et al found that octreotide promotes autophagy and attenuates LPS-induced ALI through the inhibition of AKT and mTOR phosphorylation.[46] Furthermore, Tanaka et al reported that autophagy exerts a protective effect in hyperoxia-induced lung injury.[47] Our study reveals that IRGM knockdown significantly impairs proliferation and autophagy in A549 cells, while concurrently increasing cell apoptosis and elevating levels of p-AKT and p-mTOR. These findings suggest that the protective effect of IRGM in sepsis-induced ALI is closely associated with AKT/mTOR-mediated autophagy. To further elucidate the protective mechanism of IRGM

via this signaling pathway, we employed the AKT-specific inhibitor MK2206. The findings revealed that administering the AKT inhibitor prior to the experiment reversed the detrimental effects of IRGM knockdown on LPS-induced A549 cell injury. This indicates that IRGM may enhance LPS-induced autophagy and mitigate sepsis-induced ALI by inhibiting the AKT/mTOR signaling pathway. These findings hold significant implications for future research on the protective role of IRGM in sepsis-induced ALI and for exploring novel therapeutic strategies.

In summary, our study demonstrates that IRGM enhances autophagy and prevents sepsis-induced ALI by inhibiting the AKT/mTOR signaling pathway. These findings provide new insights into the pathogenesis of sepsis-induced ALI and reveal potential strategies for the clinical management of ALI.

Data Sharing Statement

The underlying data that supports the findings of this study will be made available upon reasonable request to the corresponding author. This is done in the spirit of open science and allows others in the field to verify our results and use the data for further explorations.

Ethics Approval and Consent to Participate

The research project received approval from the Ethics Review Committee of the First Hospital of Lanzhou University (Approval number: LDYYLL2024-400).

Consent for Publication

Not Applicable.

Acknowledgments

The authors express their profound gratitude to the Experimental Animal Center of Lanzhou University for providing the equipment and space. Our appreciation also extends to the team members, without whose dedication and hard work, this study would not have been possible. We would like to thank the staff and researchers who have contributed to data collection, analysis, and interpretation, as well as the reviewers for their valuable suggestions and comments that have greatly improved the manuscript. We also acknowledge any funding bodies that have supported this work.

Funding

This study was funded by the Gansu Provincial Science and Technology Program (Project Number: 24JRRA939) and the Lanzhou Science and Technology Planning Project (2023-2-106).

Disclosure

The authors declare that they have no competing interests.

References

1. Van Der Poll T, Shankar-Hari M, Wiersinga WJ. The immunology of sepsis. *Immunity*. 2021;54(11):2450–2464. doi:10.1016/j.immuni.2021.10.012
2. Cohen J, Vincent JL, Adhikari NK, et al. Sepsis: a roadmap for future research. *Lancet Infect Dis*. 2015;15(5):581–614. doi:10.1016/S1473-3099(15)70112-X
3. Wang Y, Tang B, Li H, et al. A small-molecule inhibitor of Keap1-Nrf2 interaction attenuates sepsis by selectively augmenting the antibacterial defence of macrophages at infection sites. *EBioMedicine*. 2023;90:104480. doi:10.1016/j.ebiom.2023.104480
4. Wiersinga WJ, Van Der Poll T. Immunopathophysiology of human sepsis. *EBioMedicine*. 2022;86:104363. doi:10.1016/j.ebiom.2022.104363
5. Shi QQ, Huang YH, Li YF, et al. PEBP4 deficiency aggravates LPS-induced acute lung injury and alveolar fluid clearance impairment via modulating PI3K/AKT signaling pathway. *Cell Mol Life Sci*. 2024;81(1):133. doi:10.1007/s00018-024-05168-5
6. Deretic V. Autophagy in inflammation, infection, and immunometabolism. *Immunity*. 2021;54(3):437–453. doi:10.1016/j.immuni.2021.01.018
7. Gorman EA, O'kane CM, Mcauley DF. Acute respiratory distress syndrome in adults: diagnosis, outcomes, long-term sequelae, and management. *Lancet*. 2022;400(10358):1157–1170.
8. Liu B, Wang Z, He R, et al. Buformin alleviates sepsis-induced acute lung injury via inhibiting NLRP3-mediated pyroptosis through an AMPK-dependent pathway. *Clin Sci (Lond)*. 2022;136(4):273–289. doi:10.1042/CS20211156
9. Kitzmiller L, Ledford JR, Hake PW, et al. Activation of AMP-activated protein kinase by A769662 ameliorates sepsis-induced acute lung injury in adult mice. *Shock*. 2019;52(5):540–549. doi:10.1097/SHK.0000000000001303

10. Song L, Zhou F, Cheng L, et al. MicroRNA-34a suppresses autophagy in alveolar type II epithelial cells in acute lung injury by inhibiting FoxO3 expression. *Inflammation*. 2017;40(3):927–936. doi:10.1007/s10753-017-0537-1
11. Xu X, Li H, Gong Y, et al. Hydrogen sulfide ameliorated lipopolysaccharide-induced acute lung injury by inhibiting autophagy through PI3K/Akt/mTOR pathway in mice. *Biochem Biophys Res Commun*. 2018;507(1–4):514–518. doi:10.1016/j.bbrc.2018.11.081
12. Vishnupriya S, Priya dharshini LC, Sakthivel KM, et al. Autophagy markers as mediators of lung injury-implication for therapeutic intervention. *Life Sci*. 2020;260:118308.
13. Zhang DM, Zhang T, Wang MM, et al. TIGAR alleviates ischemia/reperfusion-induced autophagy and ischemic brain injury. *Free Radic Biol Med*. 2019;137:13–23. doi:10.1016/j.freeradbiomed.2019.04.002
14. Li Q, Ni Y, Zhang L, et al. HIF-1α-induced expression of m6A reader YTHDF1 drives hypoxia-induced autophagy and malignancy of hepatocellular carcinoma by promoting ATG2A and ATG14 translation. *Signal Transduct Target Ther*. 2021;6(1):76. doi:10.1038/s41392-020-00453-8
15. Zhao H, Chen H, Xiaoyin M, et al. Autophagy activation improves lung injury and inflammation in sepsis. *Inflammation*. 2019;42(2):426–439. doi:10.1007/s10753-018-00952-5
16. Tiwari S, Choi HP, Matsuzawa T, et al. Targeting of the GTPase Irgm1 to the phagosomal membrane via PtdIns(3,4)P(2) and PtdIns(3,4,5)P(3) promotes immunity to mycobacteria. *Nat Immunol*. 2009;10(8):907–917. doi:10.1038/ni.1759
17. Singh SB, Davis AS, Taylor GA, et al. Human IRGM induces autophagy to eliminate intracellular mycobacteria. *Science*. 2006;313(5792):1438–1441. doi:10.1126/science.1129577
18. Brest P, Lapaquette P, Souidi M, et al. A synonymous variant in IRGM alters a binding site for miR-196 and causes deregulation of IRGM-dependent xenophagy in Crohn's disease. *Nat Genet*. 2011;43(3):242–245. doi:10.1038/ng.762
19. Xu H, Wu ZY, Fang F, et al. Genetic deficiency of Irgm1 (LRG-47) suppresses induction of experimental autoimmune encephalomyelitis by promoting apoptosis of activated CD4+ T cells. *FASEB j*. 2010;24(5):1583–1592. doi:10.1096/fj.09-137323
20. He S, Wang C, Dong H, et al. Immune-related GTPase M (IRGM1) regulates neuronal autophagy in a mouse model of stroke. *Autophagy*. 2012;8(11):1621–1627. doi:10.4161/auto.21561
21. Dong H, Tian L, Li R, et al. IFNg-induced Irgm1 promotes tumorigenesis of melanoma via dual regulation of apoptosis and Bif-1-dependent autophagy. *Oncogene*. 2015;34(42):5363–5371. doi:10.1038/onc.2014.459
22. Kumar S, Jain A, Choi SW, et al. Mammalian Atg8 proteins and the autophagy factor IRGM control mTOR and TFEB at a regulatory node critical for responses to pathogens. *Nat Cell Biol*. 2020;22(8):973–985. doi:10.1038/s41556-020-0549-1
23. Kataoka Y, Shibata R, Ohashi K, et al. Omentin prevents myocardial ischemic injury through AMP-activated protein kinase- and Akt-dependent mechanisms. *J Am Coll Cardiol*. 2014;63(24):2722–2733. doi:10.1016/j.jacc.2014.03.032
24. Ding S, Qu Y, Yang S, et al. Novel miR-1958 promotes mycobacterium tuberculosis survival in RAW264.7 cells by inhibiting autophagy via Atg5. *J Microbiol Biotechnol*. 2019;29(6):989–998. doi:10.4014/jmb.1811.11062
25. Mao S, Lv J, Chen M, et al. Serinc2 deficiency causes susceptibility to sepsis-associated acute lung injury. *J Inflamm*. 2022;19(1):9. doi:10.1186/s12950-022-00306-x
26. Matute-Bello G, Downey G, Moore BB, et al. An official American thoracic society workshop report: features and measurements of experimental acute lung injury in animals. *Am J Respir Cell Mol Biol*. 2011;44(5):725–738. doi:10.1165/rcmb.2009-0210ST
27. Artham S, Gao F, Verma A, et al. Endothelial stromelysin1 regulation by the forkhead box-O transcription factors is crucial in the exudative phase of acute lung injury. *Pharmacol Res*. 2019;141:249–263. doi:10.1016/j.phrs.2019.01.006
28. Palmieri M, Pal R, Sardiello M. AKT modulates the autophagy-lysosome pathway via TFEB. *Cell Cycle*. 2017;16(13):1237–1238. doi:10.1080/15384101.2017.1337968
29. Mizushima N, Yoshimori T, Levine B. Methods in mammalian autophagy research. *Cell*. 2010;140(3):313–326. doi:10.1016/j.cell.2010.01.028
30. Park I, Kim M, Choe K, et al. Neutrophils disturb pulmonary microcirculation in sepsis-induced acute lung injury. *Eur Respir J*. 2019;53(3):1800786. doi:10.1183/13993003.00786-2018
31. Hunn JP, Feng CG, Sher A, et al. The immunity-related GTPases in mammals: a fast-evolving cell-autonomous resistance system against intracellular pathogens. *Mamm Genome*. 2011;22(1–2):43–54. doi:10.1007/s00335-010-9293-3
32. Kma L, Baruah TJ. The interplay of ROS and the PI3K/Akt pathway in autophagy regulation. *Biotechnol Appl Biochem*. 2022;69(1):248–264. doi:10.1002/bab.2104
33. Nakahira K, Cloonan SM, Mizumura K, et al. Autophagy: a crucial moderator of redox balance, inflammation, and apoptosis in lung disease. *Antioxid Redox Signal*. 2014;20(3):474–494. doi:10.1089/ars.2013.5373
34. Fan X, Wang J, Hou J, et al. Berberine alleviates ox-LDL induced inflammatory factors by up-regulation of autophagy via AMPK/mTOR signaling pathway. *J Transl Med*. 2015;13(1):92. doi:10.1186/s12967-015-0450-z
35. Dong W, He B, Qian H, et al. RAB26-dependent autophagy protects adherens junctional integrity in acute lung injury. *Autophagy*. 2018;14(10):1677–1692. doi:10.1080/15548627.2018.1476811
36. Shibutani ST, Saitoh T, Nowag H, et al. Autophagy and autophagy-related proteins in the immune system. *Nat Immunol*. 2015;16(10):1014–1024. doi:10.1038/ni.3273
37. Zhang D, Zhou J, Ye LC, et al. Autophagy maintains the integrity of endothelial barrier in LPS-induced lung injury. *J Cell Physiol*. 2018;233(1):688–698. doi:10.1002/jcp.25928
38. Li D, Li C, Wang T, et al. Geranylgeranyl diphosphate synthase 1 knockdown suppresses NLRP3 inflammasome activity via promoting autophagy in sepsis-induced acute lung injury. *Int Immunopharmacol*. 2021;100:108106. doi:10.1016/j.intimp.2021.108106
39. Arico S, Petiot A, Bauvy C, et al. The tumor suppressor PTEN positively regulates macroautophagy by inhibiting the phosphatidylinositol 3-kinase/protein kinase B pathway. *J Biol Chem*. 2001;276(38):35243–35246. doi:10.1074/jbc.C100319200
40. Lum JJ, Bauer DE, Kong M, et al. Growth factor regulation of autophagy and cell survival in the absence of apoptosis. *Cell*. 2005;120(2):237–248. doi:10.1016/j.cell.2004.11.046
41. Li Y, Xu M, Ding X, et al. Protein kinase C controls lysosome biogenesis independently of mTORC1. *Nat Cell Biol*. 2016;18(10):1065–1077. doi:10.1038/ncb3407
42. Matsuda-Lennikov M, Suizu F, Hirata N, et al. Lysosomal interaction of Akt with Phafin2: a critical step in the induction of autophagy. *PLoS One*. 2014;9(1):e79795. doi:10.1371/journal.pone.0079795

43. Manning BD, Toker A. AKT/PKB signaling: navigating the network. *Cell*. 2017;169(3):381–405. doi:10.1016/j.cell.2017.04.001
44. Glab JA, Cao Z, Puthalakath H. Bcl-2 family proteins, beyond the veil. *Int Rev Cell Mol Biol*. 2020;351:1–22.
45. Qu L, Chen C, He W, et al. Glycyrrhizic acid ameliorates LPS-induced acute lung injury by regulating autophagy through the PI3K/AKT/mTOR pathway. *Am J Transl Res*. 2019;11(4):2042–2055.
46. Zhang S, Tang C, Wang X. Octreotide activates autophagy to alleviate lipopolysaccharide-induced human pulmonary epithelial cell injury by inhibiting the protein kinase B (AKT)/mammalian target of rapamycin (mTOR) signaling pathway. *Bioengineered*. 2022;13(1):217–226. doi:10.1080/21655979.2021.2012908
47. Tanaka A, Jin Y, Lee SJ, et al. Hyperoxia-induced LC3B interacts with the Fas apoptotic pathway in epithelial cell death. *Am J Respir Cell Mol Biol*. 2012;46(4):507–514. doi:10.1165/rcmb.2009-0415OC